



Optics Letters

Tunable higher-order orbital angular momentum using polarization-maintaining fiber

BRENDAN M. HEFFERNAN,^{1,*} ROBERT D. NIEDERRITER,¹ MARK E. SIEMENS,² AND JULIET T. GOPINATH^{1,3}

¹Department of Physics, University of Colorado, Boulder, Colorado 80309, USA

²Department of Physics and Astronomy, University of Denver, 2112 East Wesley Avenue, Denver, Colorado 80308, USA

³Department of Electrical, Computer, and Energy Engineering, University of Colorado, Boulder, Colorado 80309, USA

*Corresponding author: Brendan.heffernan@colorado.edu

Received 25 April 2017; revised 10 June 2017; accepted 13 June 2017; posted 14 June 2017 (Doc. ID 294596); published 5 July 2017

For the first time, to the best of our knowledge, light with orbital angular momentum (OAM) of $\pm 2\hbar$ per photon is produced using commercially available polarization-maintaining fiber with modal purity of 96%. Twist measurements demonstrate that the average orbital angular momentum can be continuously tuned between $\pm 2\hbar$. The authors consider beams of non-integer OAM, created using the presented method, as superpositions of integer OAM states. © 2017 Optical Society of America

OCIS codes: (060.2310) Fiber optics; (060.2420) Fibers, polarization-maintaining; (080.4865) Optical vortices; (140.3300) Laser beam shaping; (260.6042) Singular optics.

<https://doi.org/10.1364/OL.42.002683>

The orbital angular momentum (OAM) of light has garnered immense interest since the seminal 1992 paper of Allen *et al.* The work showed that Laguerre–Gaussian (LG) beams have well-defined OAM of $l\hbar$, where l is the azimuthal index [1]. This has led to exciting investigations into fundamental physics such as geometric phases, spin-orbit interaction of light [2,3], and light-matter interactions [4], as well as revolutionizing understanding of photon momentum [5]. It has also been applied to a wide range of applications, including optical tweezing, micromachines, quantum computing, imaging, and information multiplexing [6,7]. The ability to generate, transport, and control OAM through optical fiber could directly advance many of these fields.

There are two main approaches to managing OAM in optical fiber. In one method, specialty fiber is designed to support OAM states as eigenmodes of the fiber by tailoring the refractive index profile [8,9]. This is important for spatial division multiplexing in communications, as OAM allows for orthogonal channels to carry information, and it is possible to propagate OAM modes over long distances with little loss or crosstalk. However, these custom fibers are not commercially available. The second method involves standard fiber, where phase-controlled combinations of fiber eigenmodes are used to construct an OAM beam at the output [10–12]. We focus on the latter approach, which can yield unique control over the

resulting light [13,14]. While OAM modes with $l = \pm 1$ have been generated using mode addition in optical fiber [10,12–14], higher-order OAM modes have not been generated. In this Letter, we demonstrate the generation of higher-order OAM modes ($l = \pm 2$).

In theory, constructing a beam with an azimuthal phase and OAM > 1 in standard step-index fiber can be achieved by coupling to HE or EH modes. Both modes have two orientations, giving rise to four total modes of interest: $\text{HE}_{L+1,m}^{\text{even}}$, $\text{HE}_{L+1,m}^{\text{odd}}$, $\text{EH}_{L-1,m}^{\text{even}}$, and $\text{EH}_{L-1,m}^{\text{odd}}$. By exciting $\text{HE}_{L+1,m}^{\text{even}}$ and $\text{HE}_{L+1,m}^{\text{odd}}$ with a relative $\pi/2$ phase difference, a beam with spin angular momentum (SAM) and OAM aligned to the same direction can be realized, resulting in stable propagation of the intensity profile along the fiber. Repeating the process with EH modes results in anti-aligned SAM and OAM, producing periodic changes in the intensity profile along propagation [15]. However, the even and odd mode orientations are completely degenerate in standard fiber, meaning even small, random perturbations to the fiber cause crosstalk and make it impractical to sustain pure optical vortices in a fiber of any significant length [8,11]. An attractive alternative is offered by polarization-maintaining fiber (PMF).

PMF has full vector eigenmodes that we represent as $\text{PM}_{lpe,o}^{s,f}$, where l is the azimuthal index, p is the radial index, “e” denotes even orientation, and “o” denotes odd. The superscript gives the polarization alignment; s represents the electric field vector along the slow axis; and f represents the fast. We assume polarization along the slow axis for the remainder of this Letter and, thus, suppress the superscript. These modes have the form

$$\text{PM}_{lpe,o} = f_{|l|p}(r) \begin{cases} \cos(l\theta) & \text{for } e \\ \sin(l\theta) & \text{for } o, \end{cases} \quad (1)$$

where θ is the azimuthal coordinate in the transverse plane of the beam, and $f_{|l|p}(r)$ describes the radial dependence of the mode. The stress rods of the PMF that create birefringence also break cylindrical symmetry and lift the degeneracy between different orientations of the same mode (including polarization), such that both orientations are stably propagated without crosstalk in 2 m of fiber. The break in symmetry is due to spatially varying stress along the transverse direction of the fiber, which

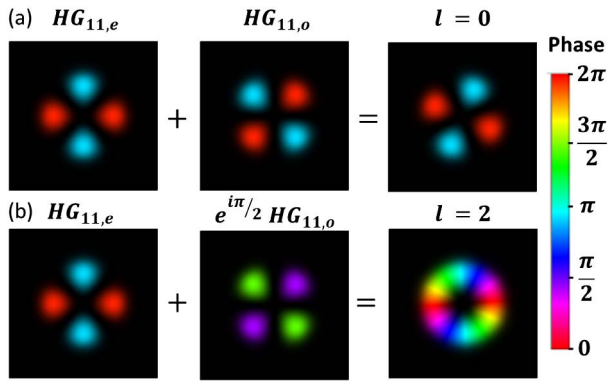


Fig. 1. Two modes supported in polarization maintaining fiber (PMF), approximated in this figure by HG modes, are added to produce a beam of either (a) OAM = 0 or (b) OAM = $\pm 2\hbar$, depending on the relative phase between modes. The color represents the phase, and the brightness represents intensity. Note that a beam of zero OAM can also be produced if the two modes are π out of phase, resulting in an intensity profile that is rotated by 45 deg from the result in (a).

causes a non-uniform refractive index distribution [16,17]. For a mode with given p and l , combining the even and odd orientations with a half-integer of π phase difference results in an azimuthal phase of the form $\exp(\pm il\theta)$. This combined mode has OAM and a topological charge of l . The $PM_{21e,o}$ modes that will be of interest for the rest of this Letter are accurately approximated by the Hermite–Gaussian (HG) modes HG_{11e} and HG_{11o} , where the first index describes the order along x and the second, y . Figure 1 demonstrates addition between these two modes.

We implement higher-order OAM generation using a 2 m long polarization-maintaining patch cord that is single-mode at 1550 nm (Thorlabs P5-1550-FC-2). At 632.8 nm, this fiber supports six modes for each linear polarization, leading to 12 total modes. In our experiment, shown in Fig. 2, fiber modes are selectively excited by generating an HG_{11o} mode using a He–Ne laser and a spatial light modulator (SLM). The beam is split into two arms, and a Dove prism is used in one of these arms to rotate the beam into the even orientation. The two beams are recombined, and a half-wave plate and polarizer balance the power between the beams and align the polarization to the slow axis of the fiber. The phase between these two modes can be finely tuned using a piezo-actuated translation stage. Additionally, the beam generated from fiber can be interfered with a Gaussian reference to qualitatively verify OAM (Fig. 2 inset). A beam of OAM $\pm 1\hbar$ can also be realized by exciting the HG_{10} and HG_{01} -like modes of the fiber, as demonstrated in [13].

Due to the large number of modes supported by the fiber, crosstalk and intermodal coupling should be considered. The stress rods of the PMF that serve to create birefringence also perturb the refractive index profile of a step index fiber. They can cause changes in the fiber modes when sufficient bending or twisting is applied [11]. Higher-order modes are particularly susceptible. Using a coupled mode theory [18–21], we can calculate the effect that a perturbation will have on modal cross talk. The matrix of coupling coefficients is given by

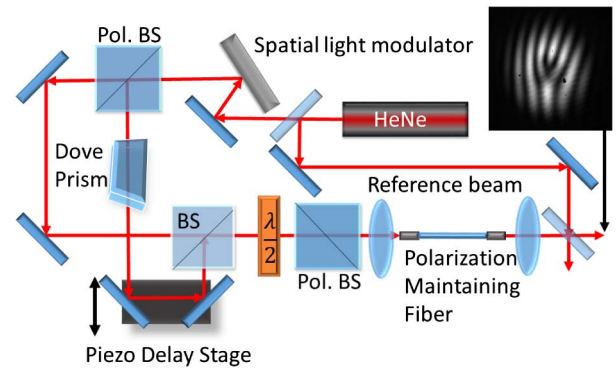


Fig. 2. Pol. BS, polarizing beam splitter; BS, beam splitter; $\lambda/2$ half-wave plate. Experimental setup. A 5 mW cw He–Ne laser at 632.8 nm is incident on a SLM. The first diffracted order is an HG_{11o} mode used to selectively excite fiber modes. A polarizing cube beam splitter is used to create a Mach–Zehnder interferometer. In one of the arms, a dove prism mounted at 22.5° rotates the excitation beam by 45° . A piezo-actuated delay stage is used to control the relative phases between the two arms before they are recombined at a 50:50 cube beam splitter. A half-wave plate is used to balance power from each arm before coupling into the PMF. The inset shows the interference between an OAM beam of $l = 2$ generated from fiber and a tilted Gaussian reference. A three-pronged “fork” is seen, indicating a phase singularity with a topological charge of 2.

$$C_{nm} = \int \delta n^2(x, y) E_n^* E_m dx dy, \quad (2)$$

where E_n is the transverse field profile of the n^{th} eigenmode of the unperturbed fiber, and $\delta n^2(x, y)$ is the change of the cross-sectional refractive index due to the perturbation defined as

$$\delta n^2(x, y) = n^2(x, y) - n_0^2(x, y), \quad (3)$$

where n is the perturbed refractive index, and n_0 is the unperturbed index.

It has been shown that a coiled fiber with a constant bending radius can be represented by a tilted refractive index profile [19,22–24]. Assuming a constant bend radius in the xz plane, this then gives the form of $n(x, y)$ as

$$n(x, y) = n_0 \left(1 + \frac{x}{R_c} \right), \quad (4)$$

where R_c is the radius of curvature.

This results in non-zero coupling coefficients between PM_{01} , PM_{21e} , and PM_{02} . Even in the case of ideal excitation of one of these modes, power can still leak into other modes. Although orthogonal orientations of the same mode (PM_{21e} and PM_{21o}) have nearly degenerate effective indices, they remain orthogonal under this index perturbation, so no power is coupled between them.

The modes of a bent fiber can also be calculated directly using the tilted refractive index [Eq. (3)]. Simulations show that beyond a radius of curvature of 50 mm, the quality of PM_{21e} begins to degrade, and there is no longer an intensity null in its center. This is consistent with experimental observations.

We mitigate the effects of mode coupling by avoiding bends of the fiber with radii of curvature smaller than ~ 50 mm, as this could easily couple power from the PM_{21e} into azimuthally

symmetric modes (such as PM_{01} or PM_{02}) with a non-zero field in the center.

To measure the OAM of the beam quantitatively, two different methods are employed: a “twist” measurement and a modal decomposition. Quantitative measurement for OAM is important for distinguishing non-integer OAM beams from one another. In our experiment, the “twist” measurement [13,14,25] is implemented by splitting the beam under test and passing each new beam through a cylindrical lens. We use two orthogonally oriented lenses to make the measurement independent of collimation. At the focus of each lens, the one-dimensional Fourier transform results in spatial separation of different momentum components transverse to the focusing axis [23]. Recording the intensity on a CCD allows the xy covariance to be calculated:

$$\langle xy \rangle = \frac{\iint I(x, y)(x - \langle x \rangle)(y - \langle y \rangle) dx dy}{\iint I(x, y) dx dy}. \quad (5)$$

$I(x, y)$ is the intensity of the beam profile at the Fourier plane and $\langle x \rangle$, $\langle y \rangle$ are the coordinates of the centroid.

The average OAM of a beam can be calculated by taking the difference of the xy covariance along the two lens axes (here assumed to be the x and y axes):

$$\langle \text{OAM} \rangle = \hbar \frac{2\pi f}{\lambda d^2} (\langle xy \rangle_x - \langle xy \rangle_y), \quad (6)$$

with f as the focal length of the cylindrical lenses and d as the distance between the lens and measurement plane. The subscripts on covariances denote the direction of focus of the lens.

The setup is calibrated with a Gaussian beam input (without OAM) and an OAM beam of $l = \pm 1$, generated with a vortex phase plate. We measure the OAM of the beam generated in fiber by continuously performing twist measurements, as the phase between the two excitation HG modes is varied with a piezo translation stage. This phase is independently measured by monitoring the fringe pattern of the two beams with a photodiode. As expected, the OAM shows smooth, sinusoidal oscillations between $\pm 2\hbar$ per photon. When the two modes have a relative phase of an integer multiple of π , the OAM is zero (Fig. 3). A pure OAM state is achieved when the two modes are added with a half-integer of π relative phase.

We are also able to control and tune beams with non-integer average OAM per photon. Non-integer OAM has been studied theoretically using spiral phase plates [26], mode-addition methods similar to those presented here [27–29], and differential operators in the Fourier domain [30]. In our system, the total beam in the LG basis is expressed as the coherent addition of two LG modes of opposite l values, meaning some portion of the photons have $\text{OAM} = 2\hbar$, while the others have $\text{OAM} = -2\hbar$. Any non-integer OAM beam generated from our fiber can be described as a weighted superposition of these two states. These superpositions can have fractional average values of OAM.

To illustrate the behavior of the average OAM beam, we examine the case of $\langle l \rangle = 1$. The intensity profile of an OAM state of $\langle l \rangle = 1$ lacks the characteristic “donut” shape of pure LG twisted light (Fig. 3). The $l = 1$ beam can be analyzed entirely in the LG basis as an unevenly weighted sum of $l = 2$ and $l = -2$ modes. The petal beam shape is due to azimuthally dependent constructive and destructive interference between modes. Note that the azimuthal phase of

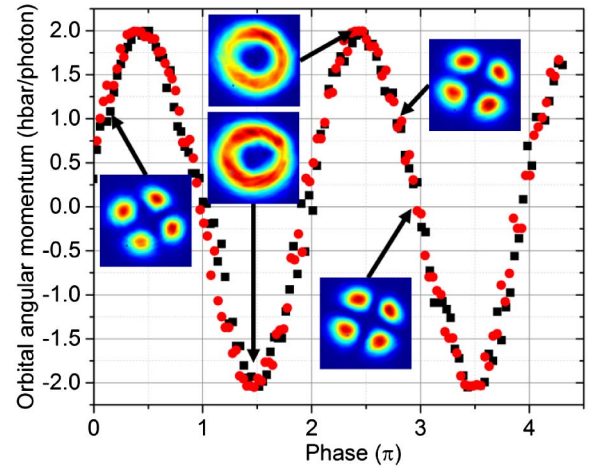


Fig. 3. Twist measurement, quantifying OAM as a function of the phase between the excitation beams. Two different trials are plotted (red circles and black squares). The maximum values demonstrate the ability to generate an OAM of $\pm 2\hbar$, while the continuous variation of OAM shows smooth control of non-integer values. These non-integer values signify the average OAM of the beam, as individual photons must have an integer \hbar of OAM. The error on each data point is estimated to be 2%.

this composite state does not increase linearly with the angle, as it would for a pure OAM state; instead, the possessing steep phase changes near the lines of minimum intensity [28]. These average OAM beams do not rotate while propagating in free space, as the phase velocity is identical for both LG modes [28,31].

For an electric field at the end of the fiber, E , an expression for the average OAM can be derived by considering the addition of the two fiber modes with a relative phase, ϕ , and expanding in the LG basis (LG_{lp}), keeping only the zeroth-order radial terms:

$$E = PM_{21}^e + \exp(i\phi) PM_{21}^o, \quad (7)$$

$$E \approx \frac{LG_{20} + LG_{-20}}{2} + \exp(i\phi) \frac{LG_{20} - LG_{-20}}{2i}, \quad (8)$$

$$E = e^{i\phi'} [-iLG_{20} \sin(\phi') + LG_{-20} \cos(\phi')], \quad (9)$$

$$\phi' = \frac{1}{2} \left(\phi + \frac{\pi}{2} \right). \quad (10)$$

Only the lowest-order radial term is considered, as the radial function of the fiber eigenmodes closely resembles that of LG modes. The power in each LG mode weights its contribution to the total OAM, so we find

$$\langle l \rangle = 2 \sin(\phi). \quad (11)$$

An alternative derivation can be attained by following [5] and integrating the angular momentum density over the entire beam.

To measure the OAM mode content, a modal decomposition measurement is performed (Fig. 4). The beam diffracts from a SLM with a forked diffraction pattern of variable l . After the SLM, a lens is used to Fourier transform the result,

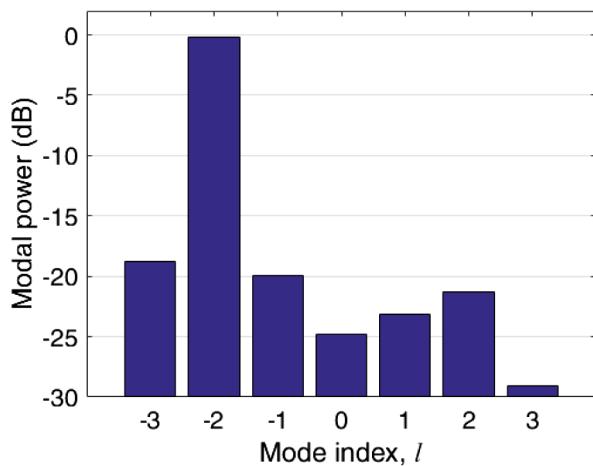


Fig. 4. Modal decomposition of an OAM beam of $l = -2$, demonstrating the ability of our method to generate high-purity optical vortices. As shown here, 96% of the power measured is contained in the $l = -2$ OAM state. These values are normalized to the total power detected.

and a CCD at the focus records the resulting intensity distribution [32]. The intensity at the centroid is measured, which is the correlation of the beam under test with a beam of OAM = $l\hbar$ [33–35]. For a given data set, these intensities are normalized by the total of intensities detected at the centroid for that set. Simulations on pure LG beams give an estimated uncertainty of 2% on the modal decomposition. For a relative phase between excitation beams of $-\pi/2$, corresponding to a generated OAM of -2 , decomposition shows that $96\% \pm 2\%$ of the power is contained in a state of $l = -2$, similar to the previous application of this mode addition method for $l = \pm 1$ [13].

The presented method for OAM generation relies on a relative phase between two modes in a fiber. External conditions, such as temperature and stress, can alter the relative phase and cause a change in OAM output. Consequently, this technique is particularly well suited for applications in fiber sensing. Under laboratory conditions, pure OAM states are stable for ~ 5 min.

In conclusion, we have demonstrated the generation of higher-order OAM in commercially available PMF. This OAM can be continuously tuned from $2\hbar$ to $-2\hbar$ per photon, and the states with maximum OAM have high modal purity. Wide tunability of OAM opens the possibility for new technologies and control of light, while the sensitivity of the relative phase between the modes of the fiber makes it a good candidate for fiber sensing.

Funding. National Science Foundation (NSF) (DMR 1553905, ECCS 1509733, ECCS 1509928, ECCS 1554704).

Acknowledgment. The authors would like to thank the staff at Coherent|Nufern for helpful technical discussions.

REFERENCES

1. M. Allen, W. Beijersbergen, R. J. C. Spreeuw, and J. P. Woerdman, *Phys. Rev. A* **45**, 8185 (1992).
2. D. L. P. Vitullo, C. C. Leary, P. Gregg, R. A. Smith, D. V. Reddy, S. Ramachandran, and M. G. Raymer, *Phys. Rev. Lett.* **118**, 083601 (2017).
3. K. Y. Bliokh, F. J. Rodríguez-Fortuño, F. Nori, and A. V. Zayats, *Nat. Photonics* **9**, 796 (2015).
4. C. T. Schmielgelow, J. Schulz, H. Kaufmann, T. Ruster, U. G. Poschinger, and F. Schmidt-Kaler, *Nat. Commun.* **7**, 12998 (2016).
5. A. T. O’Neil, I. MacVicar, L. Allen, and M. J. Padgett, *Phys. Rev. Lett.* **88**, 053601 (2002).
6. A. M. Yao and M. J. Padgett, *Adv. Opt. Photon.* **3**, 161 (2011).
7. J. Wang, M. J. Padgett, S. Ramachandran, M. P. Lavery, H. Huang, Y. Yue, Y. Yan, N. Bozinovic, S. E. Golowich, and A. E. Willner, *Optical Fiber Telecommunications VIB* (Academic, 2013), 569.
8. S. Ramachandran and P. Kristensen, *Nanophotonics* **2**, 455 (2013).
9. P. Gregg, P. Kristensen, and S. Ramachandran, *Opt. Express* **24**, 18938 (2016).
10. D. McGloin, N. B. Simpson, and M. J. Padgett, *Appl. Opt.* **37**, 469 (1998).
11. K. N. Alekseev and M. A. Yavorskiĭ, *Opt. Spectrosc.* **98**, 53 (2005).
12. S. Li, Q. Mo, X. Hu, C. Du, and J. Wang, *Opt. Lett.* **40**, 4376 (2015).
13. R. D. Niederriter, M. E. Siemens, and J. T. Gopinath, *Opt. Lett.* **41**, 3213 (2016).
14. R. D. Niederriter, M. E. Siemens, and J. T. Gopinath, *Opt. Lett.* **41**, 5736 (2016).
15. A. V. Volyar and T. A. Fadeeva, *Opt. Spectrosc.* **85**, 272 (1998).
16. M. R. Hustel and T. K. Gaylord, *App. Opt.* **51**, 5442 (2012).
17. P. Kniazewski, T. Kozacki, and M. Kujawinska, *Opt. Lasers Eng.* **47**, 259 (2009).
18. D. Marcuse, *Theory of Dielectric Waveguides* (Academic, 1974), p. 97.
19. A. W. Snyder and J. D. Love, *Optical Waveguide Theory* (Chapman & Hall, 1983), p. 467.
20. A. Yariv, *IEEE J. Quantum Electron.* **9**, 919 (1973).
21. K.-P. Ho and J. M. Kahn, *Optical Fibers Telecommunications VIB* (Academic, 2013), p. 491.
22. K. Nagano, S. Kawakami, and S. Nishida, *Appl. Opt.* **17**, 2080 (1978).
23. D. Marcuse, *Appl. Opt.* **21**, 4208 (1982).
24. C. Schulze, A. Lorenz, D. Flamm, A. Harung, S. Schröter, H. Bartelt, and M. Duparré, *Opt. Express* **21**, 3170 (2013).
25. S. N. Alperin, R. D. Niederriter, J. T. Gopinath, and M. E. Siemens, *Opt. Lett.* **41**, 5019 (2016).
26. M. V. Barry, *J. Opt. A* **6**, 259 (2004).
27. V. V. Kotlyar and A. A. Kovalev, *J. Opt. Soc. Am. A* **31**, 274 (2014).
28. A. M. Nugrowati, W. G. Stam, and J. P. Woerdman, *Opt. Express* **20**, 27429 (2012).
29. Y. Jiang, G. Ren, Y. Lian, B. Zhu, W. Jin, and S. Jian, *Opt. Lett.* **41**, 3535 (2016).
30. I. Martínez-Castellanos and J. Gutiérrez-Vega, *Opt. Lett.* **40**, 1764 (2015).
31. V. V. Kotlyar, S. N. Khonina, R. V. Skidanov, and V. A. Soifer, *Opt. Commun.* **274**, 8 (2007).
32. J. W. Goodman, *Fourier Optics* (Roberts & Company, 2005), p. 103.
33. T. Kaiser, D. Glamm, S. Schröter, and M. Duparré, *Opt. Express* **17**, 9347 (2009).
34. S. Flamm, D. Naidoo, C. Schulze, A. Forbes, and M. Duparré, *Opt. Lett.* **37**, 2478 (2012).
35. C. Schulze, A. Dudley, D. Flamm, M. Duparré, and A. Forbes, *New J. Phys.* **15**, 073025 (2013).